ISSN 0027-1349, Moscow University Physics Bulletin, 2015, Vol. 70, No. 6, pp. 497–503. © Allerton Press, Inc., 2015.
Original Russian Text © I.M. Belyaev, E.M. Govorkova, V.Yu. Egorychev, D.V. Savrina, 2015, published in Vestnik Moskovskogo Universiteta. Fizika, 2015, No. 6, pp. 68–75.

THE PHYSICS OF THE ATOMIC NUCLEUS AND ELEMENTARY PARTICLES

Study of π^0/γ Reconstruction and Selection Efficiency in the LHCb Experiment[1]

I. M. Belyaev[a], E. M. Govorkova[a, b]*, V. Yu. Egorychev[a], and D. V. Savrina[a, b]

[a] *Institute of Theoretical and Experimental Physics, National Research Centre Kurchatov Institute, Moscow, 117218 Russia*
[b] *Skobeltsyn Institute of Nuclear Physics, Moscow State University, Moscow, 119991 Russia*
**e-mail: ekaterina.govorkova@cern.ch*

Received June 29, 2015; in final form, August 12, 2015

Abstract—The reconstruction efficiency of photons and neutral pions is measured using the relative yields of reconstructed $B^+ \to J/\psi K^{*+}(\to K^+\pi^0)$ and $B^+ \to J/\psi K^+$ decays. The efficiency is studied using the data set, corresponding to an integrated luminosity of 3 fb^{-1}, collected by the LHCb experiment in proton-proton collisions at the centre-of-mass energies of 7 and 8 TeV.

Keywords: particle physics, photons, calorimeter, LHCb.
DOI: 10.3103/S0027134915060077

INTRODUCTION

The LHCb detector [1] is one of the four main experiments at the Large Hadron Collider (CERN, Geneva). The main purpose of the LHCb experiment is study of hadrons which consist of b- and c-quarks. Many of the decays under study have photons and neutral pions in the final state, for example [3–5]. The knowledge of photon reconstruction efficiency in a wide range of photon kinematic is a crucial ingredient for such kind of measurement.

The photon reconstruction efficiency is determined in data using comparison between $B^+ \to J/\psi K^+$ and $B^+ \to J/\psi K^{*+}(\to K^+\pi^0)$ signal yields. These modes are chosen, since with large branching fractions in these channels a large number of signal events is expected. The muon trigger efficiency in the experiment exceeds 90% [6], therefore, the presence of J/ψ mesons, decaying into two muons, provides high efficiency of registration of the selected decays of B mesons. Since these decays have similar topology, the large cancellation of various systematic uncertainties, after imposing similar selection and trigger criteria is expected in ratio (1). The correction factor to π^0-meson reconstruction efficiency is obtained as the following:

$$\eta_{\pi^0}^{corr} = \frac{N^{B^+\to J/\psi K^{*+}(\to K^+\pi^0)}}{N^{B^+\to J/\psi K^+}} \times \frac{\varepsilon^{MC}_{B^+\to J/\psi K^+}}{\varepsilon^{MC}_{B^+\to J/\psi K^{*+}(\to K^+\pi^0)}} \times \frac{B(B^+ \to J/\psi K^+)}{B(B^+ \to J/\psi K^{*+}(\to K^+\pi^0))}, \quad (1)$$

where N is the event yield, ε^{MC} is the total efficiency, determined using simulation, and the ratio of branching fractions is known to be [7]:

$$\frac{B(B^+ \to J/\psi K^+)}{B(B^+ \to J/\psi K^{*+}(\to K^+\pi^0))} = \left(\frac{1}{3}\times(1.39\pm0.09)\right)^{-1}. \quad (2)$$

Also the dependency of the correction factor on the transverse energy of photons and transverse momentum of π^0-mesons is studied.

1. LHCb DETECTOR

The LHCb detector is a single-arm forward spectrometer at LHC covering the pseudorapidity range $2 < \eta < 5$. In this area around 40% of all particles in production which contains b- and c-quarks are detected. The LHCb detector includes a high-preci-

[1] The article was translated by the authors.

sion tracking system consisting of vertex detector and tracking stations located upstream and downstream of a dipole magnet [2]. The tracking system provides a measurement of momentum with a relative uncertainty that varies from 0.5% at low momentum (≈500 GeV/c) to 1.0% at 200 GeV/c. Two ring-imaging Cherenkov detectors [8] are used to are distinguish between different types of charged hadrons. Calorimeter system consists of a scintillating-pad detector followed by a wall of lead and the preshower detectors, an electromagnetic calorimeter and a hadronic calorimeter. Calorimeter system is described in more details in Section 2. Muons are identified by a system composed of alternating layers of iron and multiwire proportional chambers [9].

2. THE RECONSTRUCTION OF PHOTONS

The calorimeter system performs several tasks, providing the first level trigger with high transverse momentum photon, electron and hadron candidates, measuring their energies and positions and performing the separation between photons, electrons and hadrons. To reduce number of channels readout electronics the electromagnetic calorimeter is divided into three areas: outer, middle and inner. The modules in each zone have the same design and dimensions, but differ in the number of cells per module. Thus it is considered that charging the external zone of the calorimeter is much less than loading the middle and inner zones.

The electromagnetic calorimeter employs ⟨⟨shashlik⟩⟩ technology of alternating scintillating tiles and lead plates. The energy resolution of the ECAL modules was determined at the test beam [12] and should be in agreement with the designed value $\frac{\sigma_E}{E\ (GeV)} = \frac{10\%}{\sqrt{E}} \oplus 1\%$ [14].

Energy deposits in ECAL cells are clusterized applying a 3 × 3 cell pattern around local maxima of energy deposition. Consequently the centers of the reconstructed clusters are always separated at least by one cell. Transverse energy in the local maxima is required to be more than 50 MeV. The cell with maximum energy with their neighboring cells form a cluster. If one cell is shared between several reconstructed clusters, the energy of the cell is redistributed between the clusters proportionally to the total cluster energy.

Neutral clusters are identified as those clusters that do not match to charged tracks. The tracks are extrapolated to the calorimeter surface. For each track-cluster pair two dimensional function of χ^2_{2D} is obtained, taking into account the position of the point of intersection of the extrapolated track from the calorimeter, the variance-covariance matrix of errors of this magnitude, the position of the barycenter of the cluster and the matrix of the second moments of the cluster. Cluster is identified as neutral if for all reconstructed track χ^2_{2D} is higher than 4.

The photon energy, E_c, is evaluated as follows: $E_c = \alpha \times \varepsilon_{ECAL} + \beta \times \varepsilon_{PS}$, where ε_{ECAL} is the total cluster energy, ε_{PS} is the reconstructed energy deposit in the PS. The value of parameter α depends on the position of the cluster on the calorimeter surface while β is estimated afterwards to give full account of energy samples [10, 11].

The calibration of the electromagnetic calorimeter is performed through several steps. The photoelectron multipliers gains are determined with the help of an LED system installed in the calorimeter. The final step of the calibration procedure is performed with several methods using the data coming from the experimental setup.

First the energy flow method is applied, which is based on the idea that transverse energy flow measured by the ECAL is a locally smooth function [15]. Further the calibration with neutral pions is performed. This method consists in determining the neutral pion peak position in decays of pion into two photons [20]. Only that pairs of photons, which showers do not overlap each other in the electromagnetic calorimeter are considered [16, 17]. In 2011 and 2012 precision energy recovery amounted to 2%.

3. DATA SETS

In 2011 (2012) LHCb was taking data in proton-proton collisions at a centre-of-mass energy of $\sqrt{s} = 7$ TeV (8 TeV). The collected data samples correspond to an integrated luminosity of 1 fb^{-1} in 2011 and 2 fb^{-1} in 2012. The average number of visible pp interactions per bunch crossing, μ, is 1.5 for both periods, which is four times larger than the designed value. The instantaneous luminosity, L, was increased during 2011 up to 4×10^{-32} cm^{-2} c^{-1} and during 2012 was kept constant at this value which is two times larger than the designed value. The excess of μ and L in comparison with the design values leads to higher event multiplicities, which also implies larger number of tracks and higher number of clusters in the electromagnetic calorimeter and, as consequence, higher number of overlapping clusters. Due to the difference in conditions of the data taking, the correction factors are calculated separately for 2011 and 2012 periods.

4. EVENT SELECTION

The decays $B^+ \to J/\psi K^{*+}$ followed by $K^{*+} \to K^+\pi^0$ and $B^+ \to J/\psi K^+$ are reconstructed using the $J/\psi \to \mu^+\mu^-$decay mode. The signal B^+ candidates are selected with the help of cuts applied to various kinematic parameters, particle

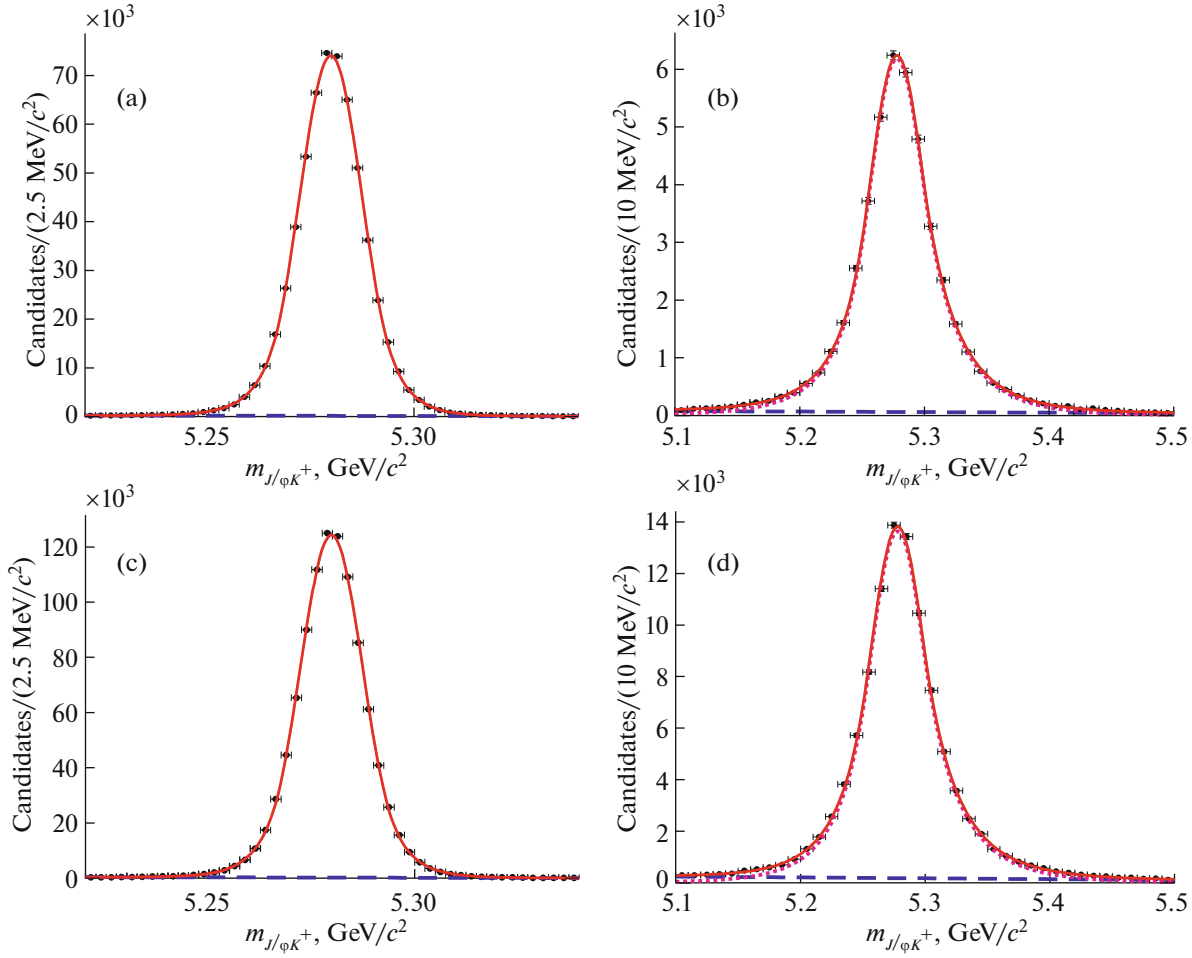

Fig. 1. Simulated mass distributions for the selected $B^+ \to J/\psi K^{*+}$ (left) and $B^+ \to J/\psi K^+$ (right) candidates (a, b) for 2011 and (c, d) 2012 data. Red curves represent the total fit function. Dashed purple and dashed blue curves represent signal and background respectively.

identification and decay reconstruction quality variables. Most selection criteria are common for the decay channels, except those which are related to the photons selection.

Pairs of oppositely-charged tracks are combined to form J/ψ candidates. The track quality of reconstructed charged particles is ensured by requiring the χ^2 per degree of freedom, provided by the track fit to be less than three, $\chi^2_{\text{tr}}/ndf < 3$. Each track should have a transverse momentum greater than 550 MeV/c and identified as muon. Well-identified muons are selected by requiring that the difference of logarithms of the muon and hadron hypothesis likelihood, provided by the particle identification detectors, is larger than zero. The invariant mass of dimuon combination is required to be around 50 MeV/c^2 of J/ψ-meson mass [7].

Photons are reconstructed using the electromagnetic calorimeter [10, 11]. For the photon identification a variable CL is used, which combines information from the calorimeter and tracking systems in order to reduce the background from hadrons, electrons and merged π^0 (those which daughter photons create largely overlapping clusters in the ECAL). The value of this variable is required to be more than 2%. The transverse momentum of the photons is required to be more than 250 MeV/c. The invariant mass of the photon pair is required to be within ±30 MeV/c^2 around the nominal π^0 mass [7].

Charged kaons are selected by requiring the transverse momentum to be in excess of 450 MeV/c. Loose kaon identification criterion is applied, the corresponding neutral network variable, P_K, is required to be greater than 0.1. The invariant mass of the $K^+\pi^0$ combinations is required to be in range ±75 MeV/c^2 around the nominal K^{*+} mass.

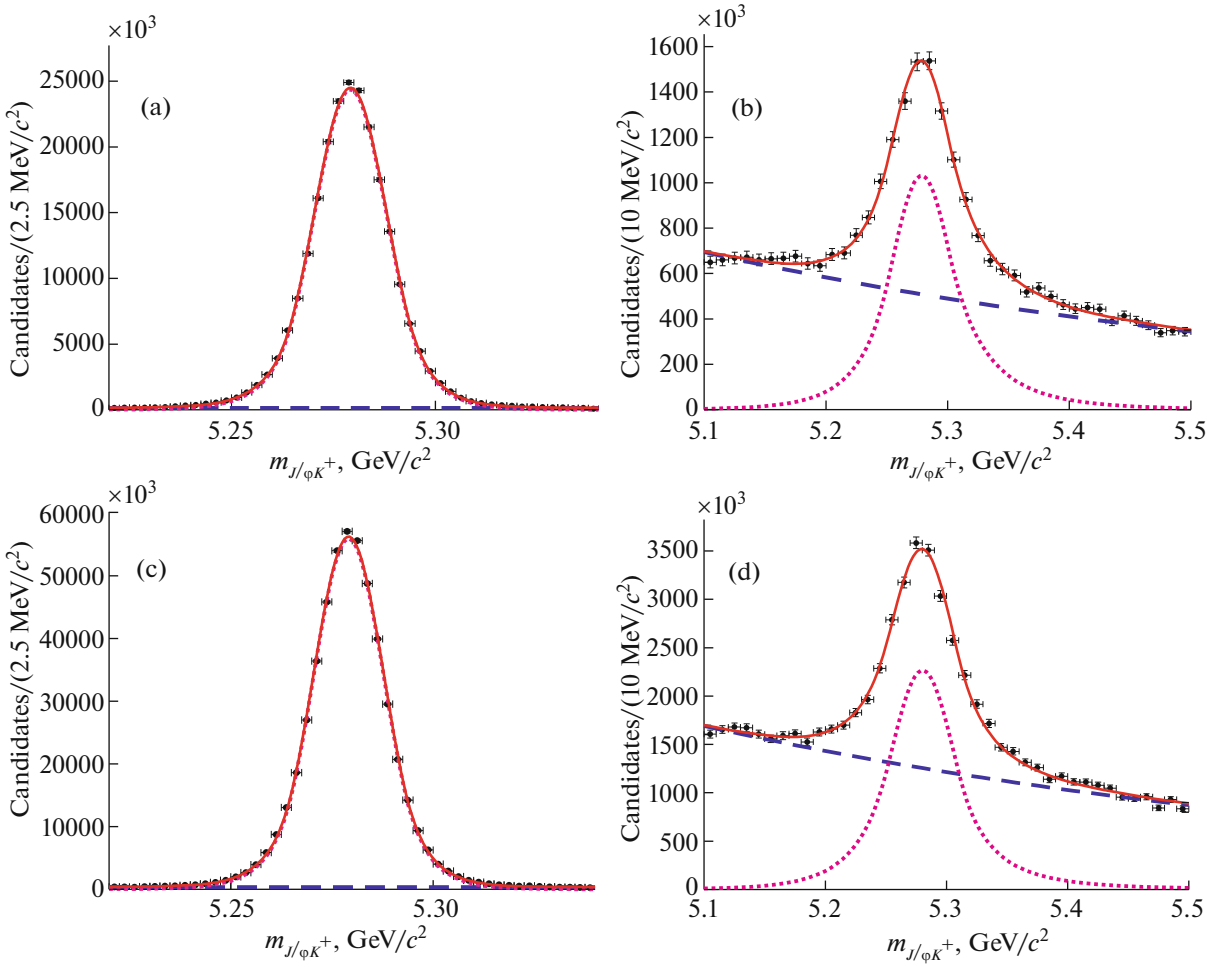

Fig. 2. Invariant mass distributions for the selected $B^+ \to J/\psi K^{*+}$ (left) and $B^+ \to J/\psi K^+$ (right) candidates (a, b) for 2011 and (c, d) 2012 data. Red curves represent the total fit function. Dashed purple and dashed blue curves represent signal and background respectively.

The B^+ candidates are formed from $J/\psi K^{(*)+}$ pairs. The transverse momentum of the B^+ candidate is required to be larger than 3 GeV/c. And the decay time of B^+ candidates is required to be in: $c\tau > 0.2$ mm. A refit of the B^+ candidate is performed taking into account primary vertex pointing constraint and J/ψ and π^0 mass constraints.

To reject possible contributions to $B^+ \to J/\psi K^{*+}$ decay from $B^+ \to J/\psi K^+$ decays with two additional random soft photons, the invariant mass of the $J/\psi K^+$combination is required to be outside a ± 25 MeV/c^2 mass window around the known B^+ mass.

5. SIGNAL YIELDS

The invariant mass distributions for the simulated $J/\psi K^+$ and $J/\psi K^{*+}$events, which have passed the selection, are shown in Fig. 1. The mass distributions for the $J/\psi K^+$ and $J/\psi K^{*+}$candidates selected from the data are shown in Fig. 2. The signal yields are determined using an extended unbinned maximum likelihood fit. The signal component for both decays is modelled by a double-sided Crystal Ball function [22]. The combinatorial background is modelled by an exponential function. For both final states the fitted position of the B^+ peak is consistent with the known B^+ mass [7] and the mass resolution is in agreement with the values observed in simulated samples. Final ratios of signal yields between $B^+ \to J/\psi K^{*+}(\to K^+\pi^0)$ and $B^+ \to J/\psi K^+$ for 2011 and 2012 data are:

$$\frac{N^{total}_{B^+\to J/\psi K^{*+}}}{N^{total}_{B^+\to J/\psi K^+}} = 0.0359 \pm 0.0009, \quad (3)$$

$$\frac{N^{total}_{B^+\to J/\psi K^{*+}}}{N^{total}_{B^+\to J/\psi K^+}} = 0.0361 \pm 0.0006. \quad (4)$$

The diphoton invariant mass distribution in data obtained using the sPlot technique [19], is shown in Fig. 3. A clear peak from the $\pi^0 \to \gamma\gamma$ decays is seen in the distribution. Its position is found to be 134.9 ± 0.1 MeV/c^2, which is consistent with the neutral π-meson mass, and the resolution is 8.3 ± 0.1 MeV/c^2.

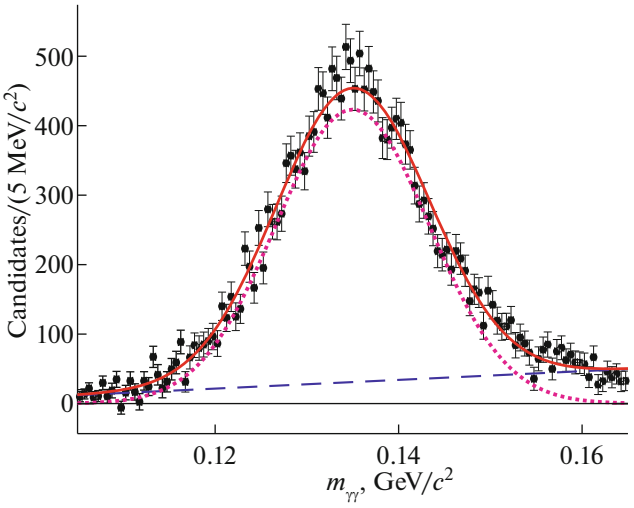

Fig. 3. Invariant mass distributions for the selected π^0 candidates.

6. EFFICIENCIES

The ratio of overall efficiencies is the product of the generator level efficiency ($\varepsilon^{gen\&acc}$) which includes the geometrical acceptance of the detector and generator level cuts efficiency, the combined reconstruction and selection efficiency ($\varepsilon^{rec\&sel}$) and the trigger efficiency (ε^{trig}). This ratio can be decomposed into three terms:

$$\frac{\varepsilon^{MC}_{B^+\to J/\psi K^+}}{\varepsilon^{MC}_{B^+\to J/\psi(K^{*+}\to K^+\pi^0)}} = \frac{\varepsilon^{gen\&acc}_{B^+\to J/\psi K^+}}{\varepsilon^{gen\&acc}_{B^+\to J/\psi(K^{*+}\to K^+\pi^0)}} \times \frac{\varepsilon^{rec\&sel}_{B^+\to J/\psi K^+}}{\varepsilon^{rec\&sel}_{B^+\to J/\psi(K^{*+}\to K^+\pi^0)}} \times \frac{\varepsilon^{trig}_{B^+\to J/\psi K^+}}{\varepsilon^{trig}_{B^+\to J/\psi(K^{*+}\to K^+\pi^0)}}. \quad (5)$$

The efficiencies and their ratios are estimated using simulation. For the simulation, pp collisions are generated using Pythia 6 and Pythia 8 [13] with a specific LHCb configuration. Decays of hadronic particles are described by EvtGen [21], in which final state radiation is generated using Photos [23]. The interaction of the generated particles with the detector and its response are implemented using the Geant4 [24, 26] toolkit. Ratios of efficiencies between $B^+ \to J/\psi K^{*+}(\to K^+\pi^0)$ and $B^+ \to J/\psi K^+$ is obtained for 2011 and 2012 data:

$$\frac{\varepsilon^{total}_{B^+\to J/\psi K^+}}{\varepsilon^{total}_{B^+\to J/\psi K^{*+}}} = 13.32 \pm 0.18, \quad (6)$$

$$\frac{\varepsilon^{total}_{B^+\to J/\psi K^+}}{\varepsilon^{total}_{B^+\to J/\psi K^{*+}}} = 13.57 \pm 0.12, \quad (7)$$

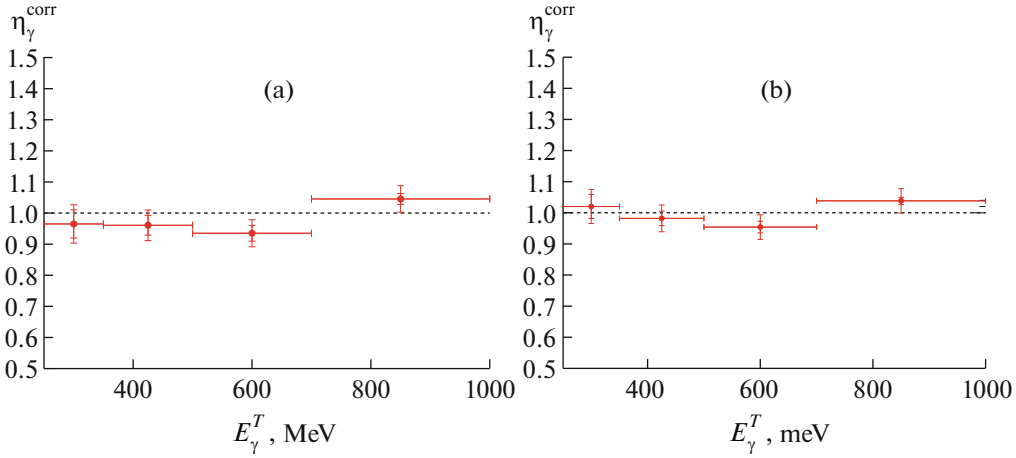

Fig. 4. Factors η_γ^{corr} for (a) 2011 and (b) 2012 data in bins of photon transverse energy.

Table 1. Relative systematic uncertainties for the correction factor of the reconstruction efficiency. The total uncertainty is the quadratic sum of the individual components

Source	Uncertainty [%]	
	2011	2012
	$\sqrt{s}$ = 7 TeV	$\sqrt{s}$ = 8 TeV
Fit model	0.2	
Trigger	1.1	
Acceptance	1.4	0.2
Total	1.8	1.1

Table 2. Factors η_γ^{corr} for 2011 and 2012 data в in bins of photon transverse energy. The first uncertainty is the statistical uncertainty, the second is systematic

E_γ^T [GeV/c]	η_γ^{corr} [%] 2011	η_γ^{corr} [%] 2012
250 – 350	$96.5 \pm 4.5 \pm 4.1$	$102.0 \pm 3.9 \pm 3.5$
350 – 500	$96.1 \pm 3.2 \pm 3.4$	$98.2 \pm 2.3 \pm 3.3$
500 – 700	$93.5 \pm 2.5 \pm 3.3$	$95.4 \pm 1.9 \pm 3.2$
> 700	$104.5 \pm 1.7 \pm 3.6$	$103.8 \pm 1.1 \pm 3.4$

where the uncertainty is due to the limited size of simulated samples.

7. SYSTEMATIC UNCERTAINTIES

Since the decay products in each channel have similar kinematic properties, most uncertainties cancel in the ratio, in particular, those related to the muon and J/ψ reconstruction and identification.

Systematic uncertainties related to the fit model are estimated using alternative models for the description of the invariant mass distributions. The following functions are used as alternative:

• a sum of a Student-t distribution with all parameters fixed from the simulation for the signal and exponent for background;

• a sum of modified Novosibirsk function [25] with all parameters fixed from the simulation for the signal and exponent for background;

• a sum of Crystall Ball function for the signal and second order polynomial for background.

For each fit model, the ratio of event yields is calculated. The maximum observed deviation from the baseline model in the ratio of yields is taken as systematic uncertainty. The obtained uncertainty is 0.2%.

The trigger efficiencies for events with J/ψ decaying into two muons produced in beauty hadron decays has been studied before [4] and a systematic uncertainty 1.1% is assigned. The uncertainty due to the limited number of simulated events vary in a range from 0.8 to 4.5%, depending on the requirements on the photon transverse energy and neutral pion transverse momentum. The corresponding systematic uncertainty is assigned in each bin of the photon transverse momentum individually.

The acceptance efficiency is calculated separately for different magnet polarities and for different data taking periods. The value of the systematic uncertainty is 1.4% for 2011 data and 0.2% for 2012 data.

The agreement between data and simulation has also been cross-checked by varying the selection criteria. No unexpectedly large deviation is found and no contribution is taken as systematics.

The contribution from $B^+ \to J/\psi\pi^+$ and $B^+ \to J/\psi\rho^+$ ($\rho^+ \to \pi^+\pi^0$) decay modes, when pion is misidentified as kaon, is found to be negligible.

The summary of systematic uncertainties is presented in Table 1. The total systematic uncertainty is 1.8% for 2011 and 1.1% for 2012.

8. CORRECTION FACTOR

The correction factor is calculated according to Eq. (1). For 2011 and 2012 data correspondingly its value is calculated to be

$$\eta_{\pi^0}^{corr}(103.2 \pm 2.6(stat) \pm 2.3(syst) \pm 6.7(B))\ \%, \quad (8)$$

$$\eta_{\pi^0}^{corr}(105.9 \pm 1.8(stat) \pm 1.6(syst) \pm 6.9(B))\ \%, \quad (9)$$

where the third uncertainty is related to an uncertainty of the known branching fractions of $B^+ \to J/\psi K^{*+}$ and $B^+ \to J/\psi K^+$ decays [7].

1. Correction Factor for Different $E^T(\gamma)$

The correction factor, η_γ^{corr}, is also studied in four bins of the photon transverse energy. The correction factors $\eta_{\pi^0}^{corr}$ can be represented as product of η_γ^{corr} for first and second photons. This leads to ten correction factors for π^0-mesons, depending on the combination of the bins, hit by the daughter photons of the π^0. The system of equations is obtained and then solved using the χ^2 method. During this procedure only statistical uncertainties are taken into account. Systematic uncertainties are evaluated using simplified simulation. The obtained values for η_γ^{corr} are shown on Fig. 2 and certain values are listed in Table 2.

2. Correction Factor for Different $p^T(\pi^0)$

The dependence of the correction factor $\eta_{\pi^0}^{corr}$ on the neutral pion transverse momentum is also studied. The transverse momentum spectra are divided into a

Table 3. Factors $\eta_{\pi^0}^{corr}$ for 2011 data in bins of neutral pion transverse momentum. The first uncertainty is the statistical uncertainty the second is systematic, and the third is related to an uncertainty of the known branching fractions of $B^+ \to J/\psi K^{*+}$ and $B^+ \to J/\psi K^+$ decays

$p_{\pi^0}^T$ [GeV/c]	$\eta_{\pi^0}^{corr}$ [%]
$0.5 - 1.0$	$93.9 \pm 7.8 \pm 2.5 \pm 6.1$
$1.0 - 1.25$	$92.1 \pm 5.0 \pm 2.4 \pm 5.9$
$1.25 - 1.5$	$94.9 \pm 4.3 \pm 2.3 \pm 6.1$
$1.5 - 2.0$	$99.5 \pm 3.2 \pm 3.7 \pm 6.4$
> 2.0	$117.2 \pm 3.7 \pm 2.6 \pm 7.6$

Table 4. Factors $\eta_{\pi^0}^{corr}$ for 2012 data in bins of neutral pion transverse momentum. The first uncertainty is the statistical uncertainty, the second is systematic, and the third is related to an uncertainty of the known branching fractions of $B^+ \to J/\psi K^{*+}$ and $B^+ \to J/\psi K^+$ decays

$p_{\pi^0}^T$ [GeV/c]	$\eta_{\pi^0}^{corr}$ [%]
$0.5 - 1.0$	$89.7 \pm 5.9 \pm 1.6 \pm 5.8$
$1.0 - 1.25$	$90.6 \pm 3.4 \pm 1.5 \pm 5.9$
$1.25 - 1.5$	$94.9 \pm 3.1 \pm 1.6 \pm 6.1$
$1.5 - 2.0$	$104.8 \pm 2.3 \pm 1.5 \pm 6.8$
> 2.0	$116.4 \pm 2.6 \pm 1.6 \pm 7.5$

few bins and the analysis is repeated for each bin separately is also studied. The transverse momentum spectra are divided into a few bins and the analysis is repeated for each bin separately. The widths of the bins are varied to allow for sufficient number of candidates in each bin. The obtained values for $\eta_{\pi^0}^{corr}$ are listed in Table 3 for 2011 data and in Table 4 for 2012 data.

CONCLUSIONS

Using data corresponding to 3 fb^{-1}, collected in 2011 and 2012 with the LHCb detector, the correction factors for the π^0 and gamma reconstruction efficiency are obtained. Their values are determined through measurement of the relative yields of $B^+ \to J/\psi K^{*+}(\to K^+\pi^0)$ versus $B^+ \to J/\psi K^+$ events. The dependency of the corrections factors on the photon transverse energy is studied.

ACKNOWLEDGMENTS

The authors thank Professor A. V. Borisov for discussion and assistance in the preparation of this article.

REFERENCES

1. A. Alves, Jr. et al. (LHCb Collab.), J. Instrum. **3**, S08005 (2008).
2. R. Arink et al. (LHCb Collab.), J. Instrum. **9**, P01002 (2014).
3. R. Aaij et al. (LHCb Collab.), Nucl. Phys. B **886**, 665 (2014).
4. R. Aaij et al. (LHCb Collab.), Nucl. Phys. B **867**, 547 (2012).
5. R. Aaij et al. (LHCb Collab.), J. High Energy Phys., No. 1, 33 (2014).
6. T. Head, J. Instrum. **9**, C09015 (2014).
7. K. A. Olive et al. (PDG Collab.), Chin. Phys. C **38**, 090001 (2014).
8. M. Adinolfi et al., Eur. Phys. J. C **73**, 2431 (2012).
9. A. Alves, Jr. et al. (LHCb Collab.), J. Instrum. **8**, P10020 (2013).
10. O. Deschamps, F. Machefert, M.-H. Schune, G. Pakhlova, and I. Belyaev, CERN-LHCb-2003-091.
11. H. Terrier and I. Belyaev, CERN-LHCb-2003-092.
12. A. Arefev, S. Barsuk, I. Belyaev, B. Bobchenko, L. Camilleri, et al., CERN-LHCB-2007-149.
13. T. Sjostrand, S. Mrenna, and P. Skands, J. High Energy Phys., No. 5, 26 (2006).
14. B. Adeva, M. Adinolfi, Z. Ajaltouni, et al., CERN-LHCC-2000-0036.
15. K. Voronchev and I. Belyaev, CERN-LHCb-2006-051.
16. A. Puig, D. Savrina, R. Graciani, and I. Belyaev, LHCb-PROC-2011-027.
17. P. Perret, arXiv:1407.4289.
18. R. Aaij et al. (LHCb Collab.), Phys. Rev. D **85**, 112013 (2012).
19. M. Pivk and F. R. Le Diberder, Nucl. Instrum. Methods Phys. Res., Sect. A **555**, 356 (2005).
20. D. Savrina and V. Egorychev, CERN-THESIS-2013-229.
21. D. J. Lange, Nucl. Instrum. Methods Phys. Res., Sect. A **462**, 152 (2001).
22. T. Skwarnicki, DESY-F31-86-02.
23. P. Golonka and Z. Was, Eur. Phys. J. C **45**, 97 (2006).
24. S. Agostinelli et al. (GEANT4 Collab.), Nucl. Instrum. Methods Phys. Res., Sect. A **506**, 250 (2003).
25. J. P. Lees et al. (BaBar Collab.), Phys. Rev. D **84**, 112007 (2011).
26. J. Allison et al. (GEANT4 Collab.), IEEE Trans. Nucl. Sci. **53**, 270 (2006).